

The OH-stretching region in infrared spectra of the apatite OH-Cl binary system

ROBERT C. TACKER¹, JOHN RAKOVAN^{2,*}, DANIEL HARLOV^{3,4,5,†}, JOHN M. HUGHES⁶, AND SARAH B. CICHY^{3,7,8}

¹North Carolina Museum of Natural Sciences, 11 West Jones Street, Raleigh, North Carolina 27612, U.S.A.

²New Mexico Bureau of Geology and Mineral Resources, Socorro, New Mexico 87801, U.S.A.

³Deutsches GeoForshungsZentrum, Telegrafenberg, Potsdam 14473, Germany

⁴Faculty of Earth Resources, China University of Geosciences, 430074 Wuhan, China

⁵Department of Geology, University of Johannesburg, P.O. Box 524, Auckland Park, 2006, South Africa

⁶Department of Geology, University of Vermont, Burlington, Vermont 05401, U.S.A.

⁷Institute for Geosciences, University of Potsdam, 14476 Potsdam-Golm, Germany

⁸Bundesgesellschaft für Endlagerung mbH (BGE), Department Site Selection, Eschenstrasse 55, 31224 Peine, Germany

ABSTRACT

Polarized Fourier transform infrared (FTIR) microspectroscopy of the OH-stretching region of hydroxylapatite-chlorapatite solid solutions presents novel problems for the assignment of peaks to specific OH-Cl pairs. Crystal structure refinements of Hughes et al. (2016) identified new positions for column anions in synthetic mixed Cl-OH apatites, with three different column anion arrangements depending on composition. These structural refinements, combined with bond-valence calculations, allow for interpretation of the OH-stretching region.

A peak at 3574 cm⁻¹ is identified as that from end-member hydroxylapatite. A second major peak at 3548 cm⁻¹ is only found in mixed chlorapatite-hydroxylapatite solid solutions, as is a third peak at 3592 cm⁻¹. Both represent perturbations of the OH-stretching vibration as compared to hydroxylapatite, to lower and higher frequency, respectively. Both of the new peaks are the result of a Cl_b-OH sequence, with adjacent anions in crystallographically similar positions, both above or both below adjacent mirror planes. One configuration has the hydrogen atom pointed toward the chlorine atom. The second has the hydrogen of the OH group pointed away from the chlorine atom.

Both configurations present novel problems. The shift to lower wavenumber at 3548 cm⁻¹ is characteristic of hydrogen bonding in fluorapatite-hydroxylapatite mixtures, yet the distance between O(H) and Cl_b is too great to allow it. The shift of OH-stretching vibrations to lower wavenumber is produced through changes in polarization of intervening Cl-Ca2' (or Ca2) and Ca2(')-O3 bonds, which are affected by the presence of the large chlorine atom. Lowering the OH-stretching vibration mimics the expected effect of chlorine on a neighboring OH group in the apatite *c*-axis column, though without hydrogen bonding. The shift to higher wavenumbers, i.e., higher frequency at 3592 cm⁻¹, is the opposite of that expected for hydrogen bonding between column anions in the apatite mineral group. It is ascribed to the interaction between an adjacent Cl_b and the oxygen end of an adjacent OH dipole. This pairing places an oxygen and a chlorine atom in close proximity. Possible means of accommodation are discussed.

A ubiquitous peak at 3498 cm⁻¹ represents hydrogen bonding between an OH and the OH_a site, with an interoxygen distance of about 2.9 Å. Published modeling supports the hypothesis that the OH_a site is occupied by an O rather than an OH. However, no clear counterpart to this pairing is observed in crystal structure refinements for specimens lacking OH_a, although the infrared absorbance is present. The existence of oxyapatite is inferred from studies of plasma-sprayed biomaterials, but the crystallographic details of the substitution have remained elusive.

A minor shoulder at 3517 cm⁻¹ does not have a clear counterpart in the structural refinements. Sequences of three columnar anions (e.g., OH-Cl-OH or Cl-OH-OH) can be ruled out, but an unequivocal assignment awaits further research.

Keywords: Apatite, solid solution, FTIR, structure refinements, hydrogen bonding, oxyapatite

INTRODUCTION

H₂O is one of the most important participants in terrestrial igneous, metamorphic, and ore-forming processes. It is incorporated into the apatite crystal structure as OH in response to variations in intensive parameters, such as the activity/fugacity of H₂O in

the environment. Chlorine is an important component of hydrous geologic fluids and an essential ligand in the mass transport of most metals. The presence of OH, halogens (F and Cl), CO₃²⁻, and SO₄²⁻ in the apatite structure provides a unique mineralogical opportunity to monitor several fluid or gaseous species simultaneously. The ubiquitous distribution of apatite allows it to be utilized in developing an extensive and internally consistent picture of fluid behavior in the Earth's crust and mantle, as well as the other terrestrial planets,

* Corresponding author E-mail: john.rakovan@nmt.edu

† Orcid https://orcid.org/0009-0009-0836-219X

moons, and meteorites.

A reliable thermodynamic model for the apatite F-OH-Cl solid solution series requires a thorough understanding of the apatite structure and how solid solution is achieved. Recent studies have revealed unexpected details about anion positions as a function of composition (Hughes et al. 2014, 2016, 2018). The expression of these structural details in infrared spectra, or as effects on the equations of state, has not yet been examined in depth. Hydrogen bonding contributes to the energetics of mixing if OH \cdots Cl and OH \cdots F pairs form in the solid solutions.

The apatite structure has been reviewed in detail (Hughes and Rakovan 2002). Fluorine, chlorine, and OH lie along the principal axis of symmetry in $P6_3/m$ apatites, coincident with the c -axis. The exact positions of the anions along the c -axis are dependent on their abundance and the concentration of their counterparts (Hughes et al. 2014, 2016). The end-members hydroxylapatite and chlorapatite are reduced in symmetry to $P2_1/b$ (first setting), as hydroxyl groups and Cl atoms are offset above or below the Ca2 triangles in single columns (which lie on mirror planes at 0 0 1/4 and 0 0 3/4), and ordered in the opposite sense in adjacent columns along b .

Routine measurement of the OH contents in apatite is complicated by problems with the measurement of F and Cl concentrations via electron microprobe, combined with subsequent assumptions of stoichiometry and charge balance on the halogen site (Goldoff et al. 2012; Stormer et al. 1993). Measurement via secondary ion mass spectrometry (SIMS) can be complicated by low-OH concentrations. Fourier transform infrared spectroscopy (FTIR) is ideal for measuring OH and H₂O in minerals, however, the OH signal in apatite is not simple (Engel and Klee 1972; Tacker 2004). The position of the OH-stretching vibration near 3572 cm⁻¹ shifts as a function of the cations in the Ca2 sites, and the position is very sensitive to anion nearest neighbors along c . This sensitivity makes FTIR an ideal tool for describing nearest-neighbor interactions and ordering in solid solutions involving hydroxylapatite.

In this study, FTIR supplements the X-ray crystal structural refinements of Hughes et al. (2016) for a set of synthetic apatites across the chlorapatite-hydroxylapatite join. Structure refinements yield a list of possible nearest neighbors among the c -axis column anion sites; FTIR shows which populations are present. The OH-stretching region provides information about the hydrogen position, which may not be discerned directly in diffraction studies (Hughes et al. 2016).

PREVIOUS WORK

Hydrogen bonding in minerals is governed by the distance between the donor oxygen and the hydrogen acceptor, as well as the electronegativity of the hydrogen acceptor (Libowitzky 1999). Both factors act on hydrogen stretching vibration. In end-member monoclinic hydroxylapatite, Ca₁₀(PO₄)₆(OH)₂, the oxygen-oxygen distance is 3.440 Å (Elliott et al. 1973), and the position of the OH-stretching vibration lies at 3572 cm⁻¹ (Tacker 2004).

Early infrared studies of fluorapatite-hydroxylapatite mixtures identified an additional OH-stretching peak at about 3535 cm⁻¹. A complete historical review is found in Elliott (1994). The X-ray structural refinements of Hughes et al. (2018) show O(H)-F interatomic distances ranging from 3.078(10) to 3.15(3) Å. This is well within the 3.2 Å limit for weak hydrogen bonding (Libowitzky 1999). The interaction of the negative fluorine

atom with the positive end of the OH dipole leads to a shift of the OH-stretching frequency from 3572 cm⁻¹ in end-member hydroxylapatite to 3535 cm⁻¹ in the F-OH apatite solid solution. This observation—hydrogen bonding with a neighboring column anion equals downshift in OH-stretching frequency—greatly influenced interpretations of the additional peaks observed in mixed Cl-OH apatites.

The addition of the larger Cl atom to hydroxylapatite was interpreted to shift the OH stretching to lower frequency, 3498 cm⁻¹ (Dykes and Elliott 1971). The greater magnitude of this shift, compared to that produced by a neighboring F (3535 cm⁻¹), was attributed to proximity rather than electronegativity (Baumer et al. 1995; Dykes and Elliott 1971; Maiti and Freund 1981). Subsequent work (Baumer et al. 1994, 1995) identified additional absorbance bands in mixed synthetic Cl-OH apatites. Baumer et al. (1994) characterized peaks at 3485, 3545, and 3498 cm⁻¹ as OH \cdots Cl pairs and 3571 cm⁻¹ as the OH-OH-OH sequence determined for hydroxylapatite. An additional band was observed at 3595 cm⁻¹, ascribed to a hydroxyl adjacent to a vacancy or from the splitting of Ca2 into two sites (Baumer et al. 1995).

X-ray crystal structure refinements of the Cl-OH mixed apatites were conducted by Hughes et al. (2016), identifying a site distinct from those found in earlier works. This site was designated ClOH and can accommodate either a Cl atom (ClOH-Cl) or an OH molecule (ClOH-OH). This additional site yields a new array of possible hydrogen-bonded pairs in the OH-Cl binary system (Hughes et al. 2016), and three different column arrangements were identified depending on composition. The different column arrangements are shown in Table 1 and in the groupings of Figure 1.

SYNTHESIS AND ANALYTICAL PROCEDURE

Synthesis

Apatites across the Cl-OH join were synthesized utilizing Cl-OH exchange between synthetic pure end-member chlorapatite and a series of Ca(OH)₂-H₂O solutions at 1100 °C and 400 MPa. Synthesis of a large size range of chlorapatite crystals up to five or more millimeters in length was achieved by dry mixing 0.03 mol (9.3 g) of Ca₅(PO₄)₃ into 0.1 mol of CaCl₂ (11 g). This mix was heated to 1375 °C in a covered Pt crucible in the open air, soaked at 1375 °C for 15 h, and then slowly cooled to 1220 at 3 °C per hour, after which the crucible was removed from the oven and air-cooled (see Schettler et al. 2011). The chlorapatite crystals were released from the flux by boiling the crystal/flux mass in 2 L of distilled H₂O, followed by 3–4 additional washings.

Apatites across the Cl-OH join were then synthesized by exchanging 400 mg of a 200–500 µm size separate of these synthetic chlorapatites with 25–200 mg of a Ca(OH)₂-H₂O solution with variable proportions of Ca(OH)₂ and H₂O. Each of the chlorapatite-Ca(OH)₂-H₂O mixes was sealed in a 4 cm long, 5 mm diameter Pt capsule and taken up to 1100 °C and 400 MPa in an internally heated gas pressure vessel using Ar as the pressure medium. Run duration was 3–6 days. The temperature was measured with three S-type thermocouples and calibrated to the melting points of NaCl at 843 °C/200 MPa and 904 °C/500 MPa (Akella et al. 1969). The accuracy is about ± 5 °C at 200 MPa and ± 20 °C at 500 MPa. Maximum thermal gradients along the capsules were ± 10 °C. Pressure measurement was done with a strain gauge and was accurate to ± 7 MPa for experiments up to 500 MPa. Pressure was controlled automatically within ± 5 MPa using the hydraulic system of the intensifier and a programmable control unit. The samples were heated isobarically with a rate of 30 °C/min and quenched isobarically with quench rates of 150–200 °C/min.

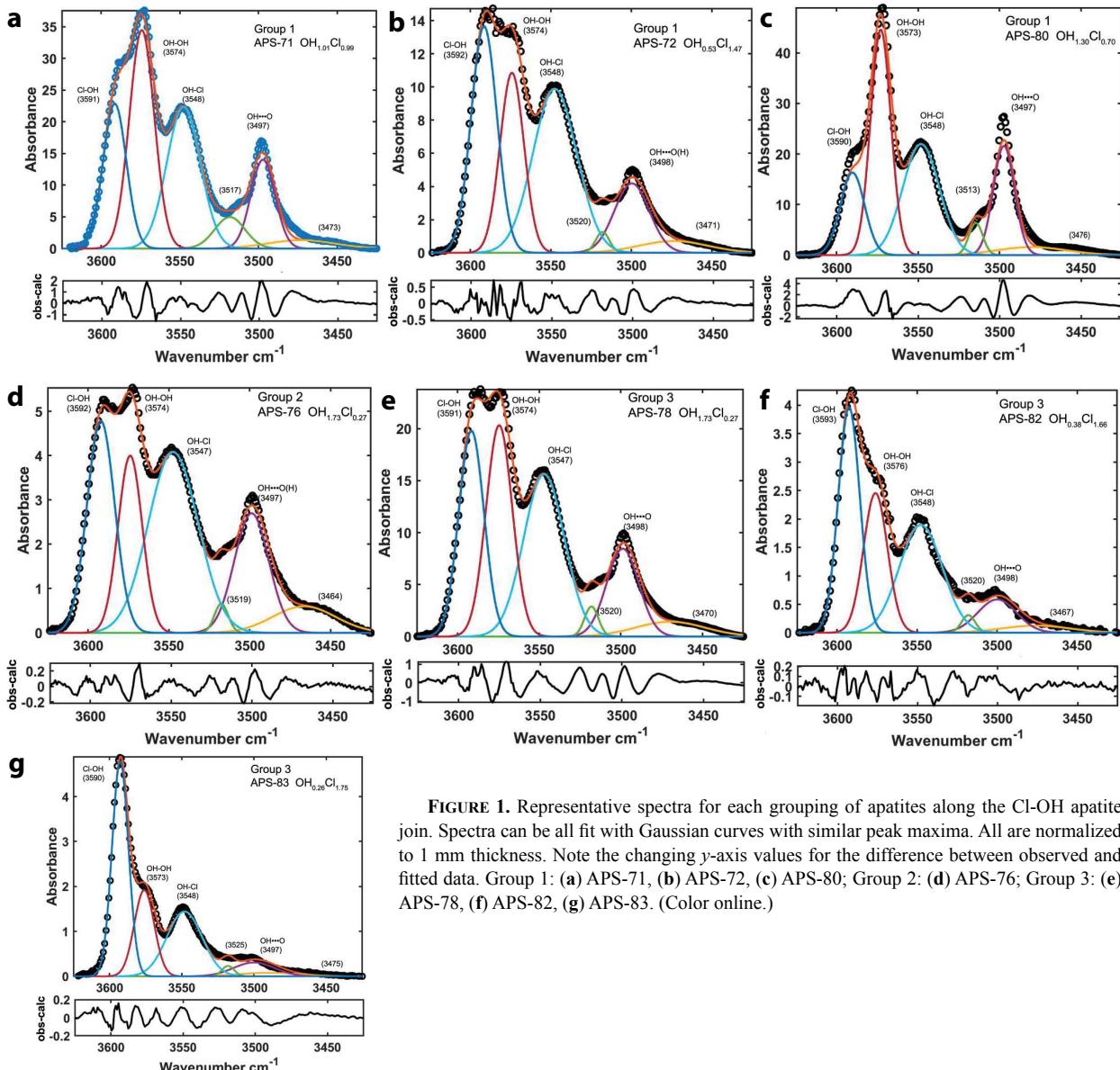
Synthesis of end-member hydroxylapatite in hydrous molten salts, [Ca(OH)₂-H₂O or Ca(OH)₂-Ca₅(PO₄)₃-H₂O] at 700–850 °C and 100 MPa total pressure in cold seal pressure vessels, was done at the North Carolina Museum of Natural Sciences. This method yielded apatites with an absorbance at 3498 cm⁻¹. Initially this was interpreted as contamination of the starting mixtures, possibly with CaCl₂, or from the dilute HCl used to separate out the apatite crystals after quenching. Starting powders were prepared again, and crystals were synthesized per the procedure outlined above. However, the 3498 cm⁻¹ absorbance was still present. Hydroxylapatite crystals were synthesized a third time from a newly ordered batch of reagent-grade Hap, Ca(OH)₂,

TABLE 1. Similarities and differences in crystallographic features of the anion column, after Hughes et al. (2016)

| | OH | OH _a | Cl _a | Cl _b | ClOH-OH | ClOH-Cl | Ca position | X _{OH} | X _{Cl} | Group |
|--------|----|-----------------|-----------------|-----------------|---------|---------|-------------|-----------------|-----------------|-------|
| APS-71 | X | | X | X | X | | Ca2' | 1.01 | 0.99 | 1 |
| APS-72 | X | | X | X | X | Ca2' | 0.53 | 1.47 | 1 | |
| APS-80 | X | | X | X | X | Ca2' | 1.30 | 0.70 | 1 | |
| APS-76 | X | | X | X | X | Ca2' | 1.73 | 0.27 | 2 | |
| APS-78 | X | | X | X | | Ca2 | 0.37 | 1.65 | 3 | |
| APS-82 | X | | X | X | | Ca2 | 0.38 | 1.66 | 3 | |
| APS-83 | X | | X | X | | Ca2 | 0.26 | 1.75 | 3 | |

Notes: The Group 1 solid solutions are lower in chlorine, and have a wider Ca²⁺ triangle to accommodate the larger chlorine atom. The Group 1 ClOH-OH site lies off the mirror plane, as does the OH in Group 3. OH_a lies at the center of the Ca²⁺ triangle. Specimen APS-76, Group 2, is somewhat intermediate to Groups 1 and 3. All three groups contain a Cl_b atom.

Ca₃(PO₄)₂, and de-ionized water. Crystals were separated from the matrix using dilute acetic acid in de-ionized water. The Pt tubing was thoroughly cleaned in HCl and then boiled several times in de-ionized water. Again, the synthesis resulted in a peak at 3498 cm⁻¹, which is examined further below.



Fourier transform infrared spectroscopy (FTIR)

FTIR measurements were conducted on a Nicolet Continuum IR microscope, with a Nicolet 6700 FTIR bench spectrometer, both from ThermoScientific. Resolution was 4 cm⁻¹. The microscope was equipped with a petrographic stage for sample orientation. Specimens were mounted in Crystal Bond, single polished, removed from the adhesive with acetone, and placed on 2 × 13 mm pre-prepared KBr disks for analysis on the petrographic stage of the IR microscope. Apatite crystals were euhedral, so the *c*-axis of the finished product was usually parallel to the stage to within a few degrees. The thickness of specimens was determined using a Mitutoyo thickness gauge to ±0.001 mm. Also used was an internal laboratory calibration of the absorbance of the phosphate combination and overtone bands between 1900 and 2300 cm⁻¹ vs. thickness [expanded from Tacker (2004)], augmented by the relationship between fringing and thickness when fringing was observed.

A ZnSe infrared polarizer was fixed in alignment with the intrinsic partial polarization of the incident radiation (Libowitzky and Rossman 1996). Polarization extinction is thus slightly better than a ZnSe polarizer alone. The OH-stretching vibration in apatite is very strongly polarized parallel to the *c*-axis, so a series of short analyses located the maximum absorbance to within 2°. The minimum absorbance was then measured normal to this direction.

A complete 180° polarized study was made of each specimen in a search for

FIGURE 1. Representative spectra for each grouping of apatites along the Cl-OH apatite join. Spectra can be all fit with Gaussian curves with similar peak maxima. All are normalized to 1 mm thickness. Note the changing y-axis values for the difference between observed and fitted data. Group 1: (a) APS-71, (b) APS-72, (c) APS-80; Group 2: (d) APS-76; Group 3: (e) APS-78, (f) APS-82, (g) APS-83. (Color online.)

possible water substitution. These studies confirmed that the OH-stretching vibration was highly polarized parallel to the *c*-axis and zero perpendicular to the maximum. Only one specimen had a non-zero component parallel to the *a*-axis, APS-76. This was attributed to the polished section sitting with the *c*-axis at an angle to the stage, which was confirmed by polarized light microscopy. In hexagonal minerals, total absorbance A_t is equal to the sum of absorbance in two mutually perpendicular directions (Libowitzky and Rossman 1996), or for these purposes, parallel to *c*- and *a*-axes, $A_t = A_{||c} + A_{||a}$. If radiation is parallel to *c* in the apatites, $A_t = A_{||c}$. For APS-76, A_t is shown.

Peak fitting was an essential part of data reduction. The OH-stretching region of the apatite group minerals is crowded with several overlapping peaks. As two peaks overlap, the apparent peak maximum is shifted toward the adjacent peak. Erroneous results are found if this overlap is not strictly accounted for. An example may be found in groundbreaking work by Baumer et al. (1985) on fluorapatite-hydroxylapatite mixtures, which have an OH-stretching peak similar to the end-member hydroxylapatite and a single peak due to hydrogen bonding with a neighboring fluorine atom. The authors found that the apparent maxima of the hydrogen-bonded peak shifted from 3538 to 3548 cm^{-1} , illustrated in their Figure 2. The lesser hypothesis is that the apparent changes in peak maxima are due to the simple additive effect produced by two overlapping peaks of changing intensity rather than any structural changes.

Peak fitting was accomplished with Matlab programs written for this purpose. Gaussian curves were used to speed computer iteration, but where small additional curves were needed for the model to converge, the models were also tested against Voigt peak shapes. Choice of peak formulation did not affect results. The wavenumber of the Gaussian maximum is taken to be the peak position.

Background correction was questioned in the review, with the assertion that it might change peak maxima. Each spectrum ($600\text{--}4000\text{ cm}^{-1}$) was corrected to a zero baseline by subtracting the lowest absorption point from the entire spectrum. Background correction for the O-H stretching region relied on a linear model with endpoints at 3400 and 3650 cm^{-1} . Results are provided in the Online Materials¹ for background correction. Linear background correction does not affect peak maxima.

RESULTS AND DISCUSSION

Earlier studies of the OH-stretching domain of synthetic Cl-OH apatites showed a combination of peaks (Baumer et al. 1994, 1995). Figure 1 shows the peaks required to successfully decompose these spectra. The entire data set of decomposed spectra has maxima, with 1 sigma error, of 3498 ± 0.85 , 3517 ± 3.6 , 3548 ± 1.08 , 3574 ± 1.4 , and $3592 \pm 0.97\text{ cm}^{-1}$. These five listed peaks are observed, in various intensities, in all the studied Cl-OH mixed apatites (Fig. 1; Online Materials¹). Assignment of peaks to specific atomic pairs is thus simplified such that each suite of mixed Cl-OH apatites will have populations with similar interatomic distances along the *c*-axis.

Assignment is constrained by consideration of the structural commonalities in the specimens studied. Table 1 gives the occupied column anion positions of the specimens, after Hughes et al. (2016). Most specimens have a Ca2' position, allowing accommodation of the larger chlorine atom. In the most chlorine-rich specimens, Ca2 positions are not split into Ca2 and Ca2'; the Ca2 triangle is simply larger to accommodate chlorine atoms. All have an OH group that is displaced from the mirror plane coincident triangle of Ca2 atoms: either a ClOH-OH group (APS-71, 72, 80), or an OH in the Cl-rich specimens (APS-76, 78, 82, 83). All specimens have a chlorine atom in the Cl_b site. Assignment of the observed spectral maxima could be limited to interactions between these anions as a starting point.

The assignment of OH and anion pairs, or OH-OH pairs, relies on several further observations. Hughes et al. (2016) found no vacancies in the structure. Anionic sequences along the *c*-axis must not be so distant as to introduce a vacancy. Evaluation of hydrogen bonding between OH and adjacent atoms, using bond-valence calculations (Brese and O'Keeffe 1991; Gagné and Hawthorne 2015) affirms that distances beyond about 3.2 \AA are too great for

hydrogen bonding to occur (Libowitzky 1999). Bond-valence calculations were used to evaluate all possible interactions between the column anions and the calcium (Ca2 or Ca2') and O atoms (O3) lining the column.

The orientation of the OH molecule with respect to the Ca2 (Ca2') triangle is an additional and important limitation. The position of the hydrogen atom was not refined in Hughes et al. (2016), but earlier crystal structural studies (Elliott et al. 1973; Hughes et al. 1989) and DFT models (de Leeuw 2002, 2010) locate the hydrogen end of the OH dipole pointing away from the adjacent Ca2 (Ca2') triangle.

The results of the constraints, as presented above, may be summarized in a single sentence: Most of the possible Cl-OH pairs and possible OH-OH pairs are either too close to be permissible or too distant to permit hydrogen bonding. The exceptions are presented below.

Assignment of the 3574 cm^{-1} absorbance

A single peak for O-H stretching at 3574 cm^{-1} is observed in end-member hydroxylapatite for infrared and laser Raman spectroscopy (Fowler 1974; Nelson and Williamson 1982). This peak is observed in all specimens (Fig. 1; Online Materials¹ Figs. OM1 and OM2). Inter oxygen distances for the OH anions along the *c*-axis have been determined to be 3.440 \AA (Elliott et al. 1973). This provides the frame of reference for OH-bearing apatites. Only O(H)-O distances below 3.2 \AA (Libowitzky 1999) will produce hydrogen bonding and shift the 3574 cm^{-1} peak for O-H stretching to lower wavenumber. Thus, the OH-OH distances in Hap are too long for hydrogen bonding, and bond-valence calculations support this. This also provides a reference for shifts to higher frequency.

Assignment of the absorbance at 3548 cm^{-1}

A peak maxima at $3548 \pm 1.08\text{ cm}^{-1}$ is found in all spectra. Exploration of O(H)-Cl distances for the group of specimens yields possible pairings of an OH and Cl_b, OH_a, and ClOH-Cl, and ClOH-OH and Cl_b, all at interatomic distances of $\sim 3.9\text{ \AA}$ (Online Materials¹ Table OM2). This is too distant for direct hydrogen bonding, yet the peak is shifted to lower wavenumbers, as compared to OH stretching in end-member Hap at 3572 cm^{-1} . This shift mimics the effects of hydrogen bonding as expected in hydroxylapatite solid solutions.

The most direct effect the chlorine atom may have on neighboring OH is via the intervening Ca2 triangle (at *z* = 0.75 in Fig. 2a) or via the Ca2' when present. The Ca2 cations are too distant for anything more than minimal influence on the O(H) atoms, for which bond valence can be calculated at $\sim 0.02\text{--}0.03$ v.u. (Gagné and Hawthorne 2015). However, the nearest O3 atom to any particular Ca2 atom lies not in the O3 triangle at *z* = 0.57, directly adjacent to the Ca2 triangle, but in the next at *z* = 0.432 (Fig. 2a). The presence of the Cl_b atom changes the polarization of the Ca2-O3 (at *z* = 0.432) bond. These changes, in turn, affect the O3-H interaction, as compared to that of end-member Hap.

The position of the hydrogen atoms was not determined in Hughes et al. (2016), but O-H distances have been determined as small as 0.92 \AA (Elliott et al. 1973) and as large as 1.08 \AA (Hughes et al. 1989). This places the hydrogen atom at 3.01 and 3.07 \AA , respectively, from the nearest O3 atoms, close enough for weak hydrogen bonding. The hydrogen is symmetrically equidistant from the three O3 atoms at *z* = 0.432 (Fig. 2a), so the weak hydrogen

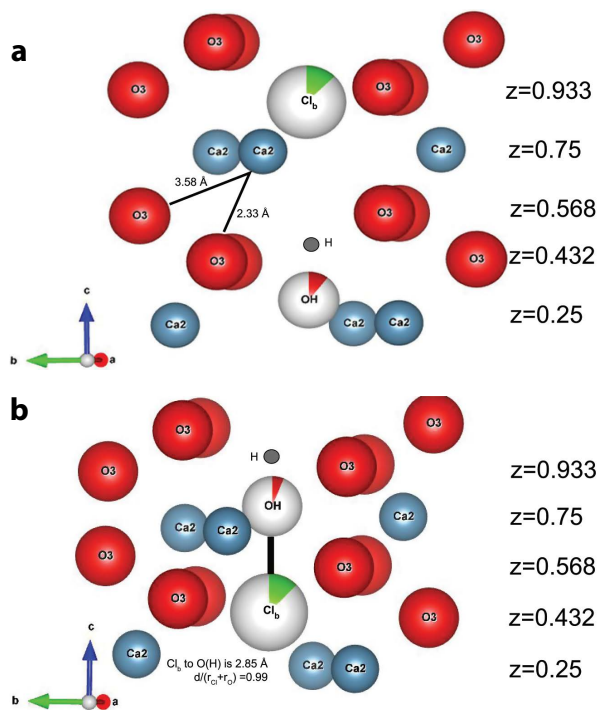


FIGURE 2. (a) “Transmission” of the effects of a Cl_b nearest neighbor to produce the peak at 3548 cm^{-1} . The Cl and OH group are too distant for hydrogen bonding, but the chlorine affects polarizability of the $\text{Ca}2$ atoms at $z = 0.75$, which in turn affects the polarization of the $\text{O}3$ atoms at $z = 0.432$. Hydrogen position is hypothetical, set at the maximum O-H distance observed for Hap (1.085 \AA ; Hughes et al. 1989), not measured. Note that the $\text{O}3$ atoms at $z = 0.432$ are closer to a $\text{Ca}2$ atom than those at $z = 0.568$. (b) “Reversed hydrogen bonding” produced by the Cl-OH pair results in a peak at higher frequency, 3592 cm^{-1} . Hydrogen position is hypothetical, at the maximum O-H distance observed for Hap (1.085 \AA ; Hughes et al. 1989), not measured. (Color online.)

bonding is multiplied by three. Hydrogen atoms at a distance of 3.01 or 3.07 \AA , respectively, from three $\text{O}3$ atoms receive a total bond valence contribution (Brese and O’Keeffe 1991) of about 1% . The net effect is to lower the O-H stretching wavenumber by 22 cm^{-1} .

The proposed origin of the O-H stretching shift may be summarized as follows. The effects of a neighboring Cl_b atom on an adjacent OH group are structural in nature, as compared to end-member Hap . Changes in the polarization of the intervening $\text{Cl-Ca}2$ ($\text{Ca}2'$) and $\text{Ca}2'(\text{-O}3)$ atoms “transmit” the presence of the chlorine atom. The shift of the O-H stretching mimics weak Cl-H hydrogen bonding even though the interatomic distance is too great.

Assignment of the absorbance at 3592 cm^{-1}

Assignment of the absorbance at 3592 cm^{-1} is more difficult because hydrogen bonding in the apatite column anions shifts a peak maximum to lower frequencies (“redshifting”), not higher. A peak absorbance at 3548 cm^{-1} is found for an OH and Cl_b pair where the hydrogen end of the dipole is pointed toward the neighboring chlorine atom (Fig. 2a). A similar sequence of $\text{Cl}_b\text{-OH}$ is possible with the hydrogen end of the dipole pointed away from the chlorine

atom (Fig. 2b). In the second case, the chlorine atom interacts with the negative end of the dipole, producing a shortened O-H bond and a shift to higher wavenumbers (“blueshifting”).

Proximity of chlorine and oxygen atoms produces something of a conundrum in terms of space requirements (interatomic distances listed in Online Materials⁴). The parameter d , interatomic distance, divided by the sum of the atomic radius of the chlorine and O atoms, should be 1 or greater, using data from Shannon (1976) for $r_{\text{Cl}} = 1.67 \text{ \AA}$ and $r_{\text{O}} = 1.20$. The $d/(r_{\text{Cl}}+r_{\text{O}})$ parameter is acceptable for the more chlorine-rich specimens in Groups 2 and 3 but ranges from 0.96 (APS-72) to 0.99 for other Group 1 specimens. Consideration of 2σ error does not improve the situation for APS-72. Specimen APS-72 exhibits a pairing of OH_a and OHCl-Cl where there is some overlap between oxygen and chlorine atoms. The OHCl-OH and Cl_b pair may predominate for APS-72.

Other details deserve consideration. The radius of the chlorine atom (Shannon 1976) is listed only for sixfold coordination. Coordination on the Cl_b site in the apatite structure is effectively threefold, and the chlorine atom will be slightly smaller.

In the literature of organic chemistry, the shift of hydrogen stretching frequency to higher wavenumbers is attributed to “anti-hydrogen bonds” (Hobza and Havlas 1999) or “blueshifted, improper hydrogen bonds” (Hobza and Havlas 2002). Reimann et al. (2001) examine the phenomenon in detail. The important difference here is the shift to higher frequency is an indirect effect of hydrogen bonding in the organic compounds. Direct interaction of the chlorine atom with the oxygen end of the OH dipole is proposed for the Cl-OH apatites.

Assignment of the 3498 cm^{-1} absorbance

Apatites specimens of Group 1 (Table 1) show a prominent absorbance between 3498 and 3500 cm^{-1} . The absorbance at 3498 cm^{-1} was initially assigned to a hydrogen-bonded OH and Cl pair (Dykes and Elliott 1971; Engel and Klee 1972; Maiti and Freund 1981), as observed in synthetic and natural Cl -bearing apatites. More recent syntheses of apatite at high temperatures (by D.H. and R.C.T.) show absorbance at the identical position yet are devoid of chlorine. Figure 3a shows the hydroxylapatite (synthesized at the North Carolina Museum of Natural Sciences) with the peak at 3498 cm^{-1} indicated. The crystal chemistry of Cl -absent apatites along the F-OH join, also synthesized at $1100 \text{ }^{\circ}\text{C}$ and 300 MPa using the technique outlined above, was described by Hughes et al. (2018). These also showed a peak at 3498 cm^{-1} . The spectra are shown in Figure 3b, with the 3498 cm^{-1} indicated. The hypothesis of OH-Cl hydrogen bonding fails. Polarized FTIR shows that the 3498 cm^{-1} vibration is polarized parallel to the c -axis as are other OH -stretching vibrations in apatite (Fig. 2a).

If hydrogen bonding with adjacent Cl is not responsible for the signal at 3498 cm^{-1} , three possibilities are suggested as nearest-neighbor hydrogen acceptors. First, the halogen site may be vacant (Schettler et al. 2011; Prener et al. 1969). Second, an H_2O molecule may have been substituted into the apatite structure (Goldenberg et al. 2015). Third, there may be an oxygen atom present on a c -axial site (Schettler et al. 2011).

The presence of a vacancy should yield an increase rather than a decrease in wavenumber, as is observed for surficial OH groups (Diallo-Garcia et al. 2014). The presence of vacancies among the column anion sites is unsupported by the data (Hughes et al.

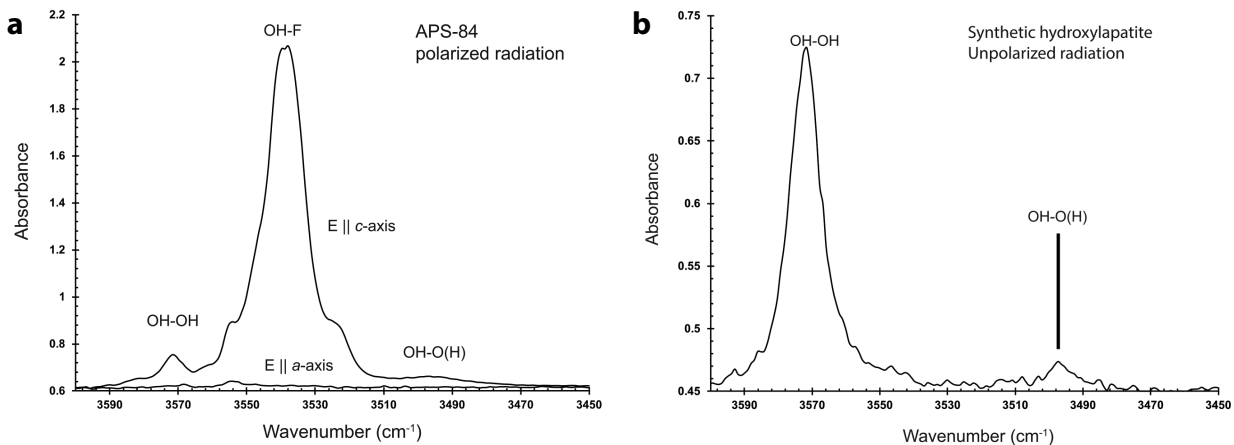


FIGURE 3. The absorbance at 3498 cm^{-1} is present in apatites that lack chlorine. (a) 3498 cm^{-1} peak in synthetic F-Hap. Polarized spectra in c -axis and a -axis directions are shown. (b) 3498 cm^{-1} peak in synthetic Hap. Crystal were too small for oriented study with polarized radiation.

2016). The lack of vacancies and the shift to lower frequency preclude the assignment of the 3498 cm^{-1} peak to a vacancy-related pairing.

If H_2O is present within the c -axis channel, it should produce two OH-stretching signals, but also an H_2O bending mode between 1590 and 1700 cm^{-1} . Water in beryl likewise occupies an axial channel and provides a structural analogy (Zhukova et al. 2014). If the longer axis of the H_2O molecule parallels the axis of symmetry, the bending mode is polarized more strongly parallel to a (Zhukova et al. 2014). Beryl has an additional sodium-linked water substitution where the bending mode is stronger parallel to c . The H_2O substitution hypothesis was tested by 180° rotation of the apatite crystal with analyses every 5 – 10° , with the c -axis parallel to the stage, using polarized radiation. Candidates for the H_2O bending mode in this region are muted and isotropic, excluding these two orientations as well as other possibilities. Furthermore, the v_3 asymmetric stretch for H_2O at $\approx 3700\text{ cm}^{-1}$ is not present (Kolesov 2006).

Least hypothesis for the peak near 3500 cm^{-1} is an OH and OH pairing shorter than that seen in end-member Hap. Group 1 specimens that have an OH_a position in the center of the Ca_2' , and in a ClOH-OH anion position, show the most prominent peaks at about 3500 cm^{-1} . Of these, a CaOH-O(H) and O(H) pair show interoxygen distances ranging from 2.76 – 2.92 \AA . Group 2 specimen, APS-76, does not have an OH_a site but has two OH groups that have a similar spacing.

Group 2 specimen APS-76 has two other off-mirror-plane OH groups that could potentially pair, OH and ClOH-OH . Interoxygen distances for this pair are 2.45 \AA . Radii for OH and O in threefold coordination are 1.20 and 1.22 \AA , respectively, (Shannon 1976), yielding a minimum atomic distance equal to the sum of the radii, or 2.40 or 2.42 \AA . Libowitzky (1999) lists interoxygen distances as low as 2.46 \AA , and Krickl and Wildner (2009) give the shortest known as 2.429 and 2.420 \AA . This short interoxygen distance was discussed by Hughes et al. (2016) and found to be acceptable.

Such a short distance would yield a strong hydrogen bond, however. The data of Libowitzky (1999) show that, at interatomic distances below about 2.85 \AA , wavenumber decreases rapidly

as interatomic distance falls. The mathematical relationship of Libowitzky (1999) predicts that an O(H)-O spacing of 2.4 \AA yields an OH-stretching vibration near 1600 cm^{-1} . The polarization test for an H_2O bending band in this region likewise rules out the short interoxygen distance.

Group 3 specimens lack a distinct OH_a site, and the 3497 cm^{-1} peak is slightly lower intensity than that of Group 1. Existing O-O distances do not permit $\text{OH}\cdots\text{OH}$, yet the peak is present, a conundrum where infrared and X-ray data do not agree. The presence of the 3497 cm^{-1} signal may indicate a minor subset of OH population, or some small differences among splits of the experimental products. These differences were not apparent in the specimens submitted for FTIR analysis.

Density function theory (DFT) models (de Leeuw et al. 2007) suggest an interesting possibility that the OH_a site would actually hold an oxygen rather than an OH. The data of Hughes et al. (2016) allows this possibility as it did not resolve the hydrogen atoms. An interesting implication of this assignment is that it solves the crystallographic details of oxyapatite substitution and provides a means through which the presence of $\text{OH}\cdots\text{O}$ hydrogen bonding may be identified in plasma-sprayed Hap powders. Oxyapatite is accepted as forming during high-temperature dehydration of hydroxylapatite powders during plasma-spraying (Gross et al. 1998; Hartmann et al. 2001).

Independent infrared spectroscopic support for this $\text{OH}\cdots\text{O}$ peak assignment is lacking. Zhou et al. (1993) studied changes in Hap with heating and showed a peak at lower frequencies than 3570 cm^{-1} that is potentially an OH paired with oxygen. In other studies, the peak position is commonly obscured by a broad absorbance related to H_2O (e.g., Yu et al. 2007) resulting from the use of Nujol or KBr pressed pellets, which are hydroscopic. Many studies relied on attenuated total reflectance (ATR) methods, far less sensitive to the OH-stretching region than the microanalytical methods used in this study.

Definitive support for oxyapatite, with oxygen in the OH_a site, is not available from other lines of inquiry. Electron paramagnetic resonance (EPR) spectroscopy has readily identified an oxygen hole-like defect on the hexad in natural apatite (Gilinskaya 2001), Hap (Ishchenko et al. 2009), and in Clap (Nokhrin et al.

2005), but do not reveal the position along the *c*-axis. Alberius-Henning et al. (1999, 2001) show a reduction in symmetry for partially hydroxylated Hap, with the oxygen near the center of the Ca₂ triangle or slightly off the plane of the triangle, but these results were reached with Rietveld analysis rather than single-crystal structural analysis. Hartmann et al. (2001) present intriguing NMR data that shows an additional hydrogen population developing in heat-treated Hap (an OH···O population?), but unfortunately, the infrared spectra cut off above 1500 cm⁻¹.

However, oxygen in an OH_a position may serve a more fundamental role in stabilizing the apatite structure and providing charge balance. Certainly, it is frequently observed in natural apatites (Tacker 2004). In hydroxyl-rich apatites, it may serve to stabilize the hexagonal structure by reversing the ordering of the hydroxyl ions above or below the mirror plane, which is essential to the monoclinic structure. Assignment of the 3498 cm⁻¹ absorbance to an OH···O pair hints at a tool for studying its occurrence in plasma-sprayed biomaterials.

Data in hand show that the 3498 cm⁻¹ is best explained by an OH anion hydrogen bonded to another OH in the OH_a site at a distance of about 2.9 Å. The presence of an oxygen atom without hydrogen in the OH_a site is intriguing but awaits further inquiry.

Assignment of the 3519 cm⁻¹ peak

The final peak at about 3519 cm⁻¹ is a minor absorbance, or a shoulder, and does not have a clear counterpart in the crystallographic refinements. The peak fitting model does not approximate this peak very well, sometimes shifting the peak position to the non-zero space at slightly higher wavenumbers. The addition of another peak in this region would improve the fit, but there is no justification for doing so. The maximum mismatch for the area around the 3519 cm⁻¹ peak is 2 absorbance units (Fig. 1). In the end, it was preferable to have a small mismatch rather than introduce spurious peaks to the model.

The calibration of Libowitzky (1999) predicts an O-O distance of 2.926 Å. The calibrations of Mikenda (1986) and Mikenda and Steinböck (1996) predict an interatomic O-Cl distance of 3.371 and 3.374 Å, respectively. Spacing of ~3.45 Å in apatite is that of anions in structurally equivalent positions along the *c*-axis. This would also apply to anions in the ClOH site.

Interatomic spacing for the ClOH sites, hosting chlorine or OH, is slightly greater than predicted from the Mikenda (1986) and Mikenda and Steinböck (1996) calibrations and, again, greater than the 3.2 Å limit on hydrogen bonding. Structural control of the changes to the O-H vibration would be similar to those ascribed to the 3548 cm⁻¹ vibration, that is, changes in the Ca-Cl_a or Ca-Cl_b dipole would affect changes on the Ca-O3 dipole for the O3 triangle surrounding the H atom.

Yet assignment of the absorbance to this pair of anions is possible for the Group 1 and Group 2 specimens but not for Group 3. To apply this assignment across the data set would require the presence of a ClOH site in specimens where it was not observed via X-ray, or an amount of heterogeneity among the specimens that is not supported by the FTIR data.

There is a possibility that the 3517 cm⁻¹ represents three column anions in sequence along the *c*-axis, for example, OH-Cl-OH or Cl-OH-Cl. This hypothesis is testable by bond-valence calculations, and the viability of these sequences is

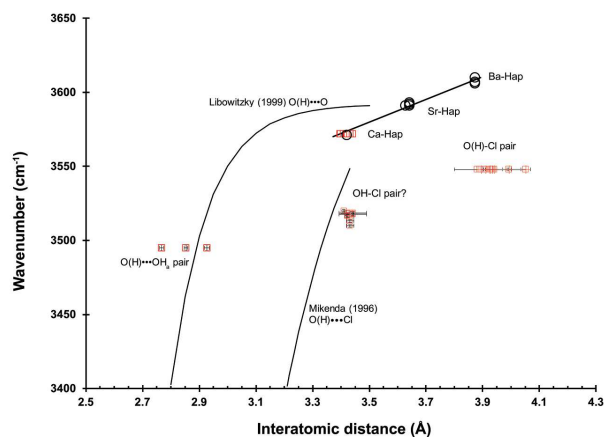


FIGURE 4. Comparison of present data with earlier work. The calibrations shown are for OH-stretching frequency vs. interatomic distance for O(H)···O (Libowitzky 1999), and for O(H)···Cl (Mikenda 1986; Mikenda and Steinböck 1996). One sigma error is shown. Results of earlier studies are shown in open circles for calcium hydroxylapatite (Fowler 1974), strontium hydroxylapatite (Collin 1959; Engel and Klee 1972; Fowler, 1974; Frangopol et al. 2016), and barium hydroxylapatite (Engel and Klee 1972; Fowler 1974; Yasukawa et al. 2005). (Color online.)

precluded by anionic size or distance. Ultimately, the assignment of the 3517 cm⁻¹ peak is left open until more data are available.

IMPLICATIONS

Comparison of results with earlier studies (Fig. 4) of OH-stretching frequency vs. distance [O(H)···O (Libowitzky 1999), or for O(H)···Cl (Mikenda 1986; Mikenda and Steinböck 1996)] further suggests that direct hydrogen bonding is not the principle control in the OH-stretching region for Cl-OH apatite mixtures. The O(H)···O(H) pair at 3498 cm⁻¹ is the only one to compare well with Libowitzky's (1999) calibration (Fig. 4).

The peak shift to higher wavenumbers, producing the 3591 cm⁻¹ peak, is the result of interaction between the oxygen end of the OH dipole and a neighboring chlorine atom. To avoid confusion with the earlier terms, “anti-hydrogen bonds” and “improper, blueshifting hydrogen bonds,” the term “inverted hydrogen bonding” is suggested. Future studies could exploit neutron diffraction to identify the hydrogen atom position. Solid-state proton nuclear magnetic resonance spectroscopy may assist in testing for the presence of a shorter O-H bond.

The frequency of the OH-stretching vibration increases with increasing unit-cell size of these three end-members, calcium hydroxylapatite (Fowler 1974), strontium hydroxylapatite (Collin 1959; Engel and Klee 1972; Fowler 1974; Frangopol et al. 2016); and barium hydroxylapatite (Engel and Klee 1972; Fowler 1974; Yasukawa et al. 2005). Fowler (1974) attributed the differences to possible changes in the PO₄ group, which is bonded to two O3 atoms (above and below the mirror plane), lining the sixfold axial channel. Our mechanism for a decrease in OH-stretching wavenumbers relies instead on changes in the Ca₂(*i*) triangle and its closest O3 atom. Changes in polarization resulting from different size cations should be considered, but our mechanism may apply to the spectra of Ca-Hap, Sr-Hap, and Ba-Hap as well.

The peak at 3548 cm^{-1} has been recognized (Tacker 2004) but not properly assigned. Originally, the best match was a configuration of 3Sr-OH-F or 3Mn-OH-OH (three cations substituted in the Ca_2 site), suggesting that the cations were not distributed randomly in the Ca positions. Correct attribution as a $3\text{Ca}_2\text{-OH-Cl}$ configuration negates these difficulties.

The possible presence of $\text{OH}\cdots\text{O}$ pairs requires a reassessment of assumptions of stoichiometry in the column anion sites. The area of the 3498 cm^{-1} peak represents 2–15% of the total area of the OH-stretching region in the spectra presented herein. Spectra from this study show that as much as 15% of OH calculated from assumed stoichiometry ($X_{\text{OH}} = 1 - X_{\text{F}} + X_{\text{Cl}}$) may actually be oxygen. As discussed above, crystal structure data (Hughes et al. 2016) do not permit vacancies, so the charge-balance mechanism remains somewhat enigmatic. A realistic expression for normalized stoichiometry on the sixfold axial site for natural apatites includes oxygen, carbonate, and vacancies, where $1 = X_{\text{F}} + X_{\text{Cl}} + X_{\text{OH}} + X_{\text{O}} + X_{\text{A Type CO}_3} + X_{\square}$, X is mole fraction and \square is a vacancy [see Schettler et al. (2011) for discussion of vacancies].

The data also suggest that curve fitting methods for natural ternary (OH-Cl-F) apatites require close attention to detail. The peaks at 3548 and 3517 cm^{-1} flank a prominent OH-F band at 3535 cm^{-1} in natural apatites and may be obscured. Two observations simplify the process. First, peak maxima positions for the apatite OH-stretching domain are quite consistent. Second, peak fitting relies on an assumption of peak symmetry, so statistical tests of skewness are appropriate. Peak broadening is a common feature in apatite spectra, especially those produced at low temperatures, but apatite crystals from igneous and metamorphic sources can be expected to be far more crystalline and possess better long-range ordering than do low-temperature precipitates.

ACKNOWLEDGMENTS AND FUNDING

Our thanks to Eugen Libowitzky and an anonymous reviewer for their thorough reviews. This research was supported by the National Science Foundation in the form of grants EAR-0910902 and EAR-0929898, both to R.C.T. Additional grant support was supplied by the Friends of the North Carolina Museum of Natural Sciences. R.C.T. gratefully acknowledges the patience of his co-authors as he went through multiple rounds of surgery and recovery.

REFERENCES CITED

Akella, J., Vaidya, S.N., and Kennedy, G.C. (1969) Melting of sodium chloride at pressures to 65 kbar. *Physical Review*, 185, 1135–1140, <https://doi.org/10.1103/PhysRev.185.1135>.

Alberius-Henning, P., Landa-Cánovas, A.R., Larsson, A.K., and Lidin, S. (1999) Elucidation of the crystal structure of oxyapatite by high-resolution electron microscopy. *Acta Crystallographica Section B*, 55, 170–176, <https://doi.org/10.1107/S0108768198012798>.

Alberius-Henning, P., Adolfsson, E., Grins, J., and Fitch, A. (2001) Triclinic oxy-hydroxyapatite. *Journal of Materials Science*, 36, 663–668, <https://doi.org/10.1023/A:1004876622105>.

Baumer, A., Ganteaume, M., and Klee, W.E. (1985) Determination of OH ions in hydroxyfluorapatites by infrared-spectroscopy. *Bulletin de Minéralogie (Paris)*, 108, 145–152, <https://doi.org/10.3406/bulmi.1985.7864>.

Baumer, A., Guilhot, B., Gilbert, R., Vernay, A.M., and Ohnenstetter, D. (1994) Characterization by infrared spectrometry of chlorine and fluorine ions in apatites. *Comptes Rendus de L'Academie Des Sciences Serie II*, 319, 193–200.

Baumer, A., Gilbert, R., Vernay, A.M., and Lapraz, D. (1995) Incorporation of hydroxyl ions into chlorapatite—Characterization by infrared spectrometry (Diffuse-reflectance). *Comptes Rendus De L'Academie Des Sciences Serie II Fascicule a-Sciences De La Terre et Des Planètes*, 321, 579–584.

Brese, N.E. and O'Keeffe, M. (1991) Bond-valence parameters for solids. *Acta Crystallographica Section B*, 47, 192–197, <https://doi.org/10.1107/S0108768190011041>.

Collin, R.L. (1959) Strontium calcium hydroxyapatite solid solutions—preparation and lattice constant measurements. *Journal of the American Chemical Society*, 81, 5275–5278.

de Leeuw, N.H. (2002) Density function theory calculations of local ordering of hydroxy groups and fluoride ions in hydroxyapatite. *Physical Chemistry Chemical Physics*, 4, 3865–3871, <https://doi.org/10.1039/b203114k>.

— (2010) Computer simulations of structures and properties of the biomaterial hydroxyapatite. *Journal of Materials Chemistry*, 20, 5376–5389, <https://doi.org/10.1039/b921400c>.

de Leeuw, N.H., Bowe, J.R., and Rabone, J.A.L. (2007) A computational investigation of stoichiometric and calcium-deficient oxy- and hydroxy-apatites. *Faraday Discussions*, 134, 195–214, discussion 215–33, 415–9, <https://doi.org/10.1039/B602012G>.

Diallo-García, S., Ben Osman, M., Krafft, J.-M., Boujday, S., and Guyène, C. (2014) Discrimination of infrared fingerprints of bulk and surface POH and OH of hydroxyapatites. *Catalysis Today*, 226, 81–88, <https://doi.org/10.1016/j.cattod.2013.11.041>.

Dykes, E. and Elliott, J.C. (1971) The occurrence of chloride ions in the apatite lattice of Holly Springs hydroxyapatite and dental enamel. *Calcified Tissue Research*, 7, 241–248, <https://doi.org/10.1007/BF02062611>.

Elliott, J.C. (1994) Structure and Chemistry of the Apatites and Other Calcium Orthophosphates. *Studies in Inorganic Chemistry*, 1st ed., 404 p. Elsevier.

Elliott, J.C., Mackie, P.E., and Young, R.A. (1973) Monoclinic hydroxyapatite. *Science*, 180, 1055–1057, <https://doi.org/10.1126/science.180.4090.1055>.

Engel, G. and Klee, W.E. (1972) Infrared-spectra of hydroxyl ions in various apatites. *Journal of Solid State Chemistry*, 5, 28–34, [https://doi.org/10.1016/0022-4596\(72\)90004-7](https://doi.org/10.1016/0022-4596(72)90004-7).

Fowler, B.O. (1974) Infrared studies of apatites. 1. Vibrational assignments for calcium, strontium, and barium hydroxyapatites utilizing isotopic-substitution. *Inorganic Chemistry*, 13, 194–207, <https://doi.org/10.1021/ic50131a039>.

Frangopol, P.T., Mocanu, A., Almasan, V., Garbo, C., Balint, R., Borodi, G., Bratu, I., Horovitz, O., and Tomoaia-Cotisel, M. (2016) Synthesis and structural characterization of strontium substituted hydroxyapatites. *Revue Roumaine De Chimie*, 61, 337–344.

Gagné, O.C. and Hawthorne, F.C. (2015) Comprehensive derivation of bond-valence parameters for ion pairs involving oxygen. *Acta Crystallographica Section B, Crystal Engineering and Materials*, 71, 562–578, <https://doi.org/10.1107/S2052520615016297>.

Gilinskaya, L.G. (2001) ESR of OH—O—OH— centers in natural apatites. *Journal of Structural Chemistry*, 42, 317–377, <https://doi.org/10.1023/A:1012400702572>.

Goldenbeld, J.E., Wilk, Z., Schermerhorn, D.V., Pasteris, J.D., and Yoder, C.H. (2015) Structural effects on incorporated water in carbonated apatites. *American Mineralogist*, 100, 274–280, <https://doi.org/10.2138/am-2015-5025>.

Goldoff, B., Webster, J.D., and Harlov, E.D. (2012) Characterization of fluor-chlorapatites by electron probe microanalysis with a focus on time-dependent intensity variation of halogens. *American Mineralogist*, 97, 1103–1115, <https://doi.org/10.2138/am.2012.3812>.

Gross, K.A., Berndt, C.C., Stephens, P., and Dinnebier, R. (1998) Oxyapatite in hydroxyapatite coatings. *Journal of Materials Science*, 33, 3985–3991, <https://doi.org/10.1023/A:1004605014652>.

Hartmann, P., Jager, C., Barth, S., Vogel, J., and Meyer, K. (2001) Solid State NMR, X-ray diffraction, and infrared characterization of local structure in heat-treated oxyhydroxyapatite microcrystals: An analog of the thermal decomposition of hydroxyapatite during plasma spray procedure. *Journal of Solid State Chemistry*, 160, 460–468, <https://doi.org/10.1006/jssc.2001.9274>.

Hobza, P. and Havlas, Z. (1999) The fluoroform···ethylene oxide complex exhibits a C—H···O anti-hydrogen bond. *Chemical Physics Letters*, 303, 447–452, [https://doi.org/10.1016/S0009-2614\(99\)00217-1](https://doi.org/10.1016/S0009-2614(99)00217-1).

— (2002) Improper, blue-shifting hydrogen bond. *Theoretical Chemistry Accounts*, 108, 325–334, <https://doi.org/10.1007/s00214-002-0367-5>.

Hughes, J.M. and Rakovan, J. (2002) The crystal structure of apatite, $\text{Ca}_5(\text{PO}_4)_3(\text{FOH},\text{Cl})$. *Reviews in Mineralogy and Geochemistry*, 48, 1–12.

Hughes, J.M., Cameron, M., and Crowley, K.D. (1989) Structural variations in natural F, OH, and Cl apatites. *American Mineralogist*, 74, 870–876.

Hughes, J.M., Nekvasil, H., Ustunisik, G., Lindsley, D.H., Coraor, A.E., Vaughn, J., Phillips, B.L., McCubbin, F.M., and Woerner, W.R. (2014) Solid solution in the fluorapatite-chlorapatite binary system: High-precision crystal structure refinements of synthetic F-Cl apatite. *American Mineralogist*, 99, 369–376, <https://doi.org/10.2138/am.2014.4644>.

Hughes, J.M., Harlov, D., Kelly, S.R., Rakovan, J., and Wilke, M. (2016) Solid solution in the apatite OH-Cl binary system: Compositional dependence of solid-solution mechanisms in calcium phosphate apatites along the Cl-OH binary. *American Mineralogist*, 101, 1783–1791, <https://doi.org/10.2138/am-2016-5674>.

Hughes, J.M., Harlov, D., and Rakovan, J. (2018) Structural variations along the apatite F-OH join. *American Mineralogist*, 103, 1981–1987, <https://doi.org/10.2138/am-2018-6608>.

Ishchenko, S.S., Vorona, I.P., Baran, N.P., Okulov, S.M., and Rudko, V.V. (2009) Thermally induced changes of the carbonate structure in biological hydroxyapatite studied by EPR and ENDOR. *Ukrainian Journal of Physics*, 54, 231–237.

Kolesov, B.A. (2006) Raman spectra of single H_2O molecules isolated in cavities of crystals. *Journal of Structural Chemistry*, 47, 21–34, <https://doi.org/10.1007/s10947-006-0261-4>.

Krickl, R. and Wildner, M. (2009) Crystal chemistry of synthetic Co- and Ni-analogues of natrochalcite—the shortest known hydrogen bonds among mineral-type compounds. Part II: Spectroscopic studies. *European Journal of Mineralogy*, 21, 65–78, <https://doi.org/10.1016/j.ejm.2008.11.001>.

doi.org/10.1127/0935-1221/2009/0021-1859.

Libowitzky, E. (1999) Correlation of O-H stretching frequencies and O-H···O hydrogen bond lengths in minerals. *Monatshefte für Chemie*, 130, 1047–1059, <https://doi.org/10.1007/BF03354882>.

Libowitzky, E. and Rossman, G.R. (1996) Principles of quantitative absorbance measurements in anisotropic crystals. *Physics and Chemistry of Minerals*, 23, 319–327.

Maiti, G.C. and Freund, F. (1981) Incorporation of chlorine into hydroxyapatite. *Journal of Inorganic and Nuclear Chemistry*, 43, 2633–2637, [https://doi.org/10.1016/0022-1902\(81\)80589-1](https://doi.org/10.1016/0022-1902(81)80589-1).

Mikenda, W. (1986) Stretching frequency versus bond distance correlation of O–D(H)···Y (Y = N, O, S, Se, Cl, Br, I) hydrogen bonds in solid hydrates. *Journal of Molecular Structure*, 147, 1–15, [https://doi.org/10.1016/0022-2860\(86\)87054-5](https://doi.org/10.1016/0022-2860(86)87054-5).

Mikenda, W. and Steinböck, S. (1996) Stretching frequency vs. bond distance correlation of hydrogen bonds in solid hydrates: A generalized correlation function. *Journal of Molecular Structure*, 384, 159–163, [https://doi.org/10.1016/S0022-2860\(96\)09335-0](https://doi.org/10.1016/S0022-2860(96)09335-0).

Nelson, D.G.A. and Williamson, B.E. (1982) Low-temperature laser Raman-spectroscopy of synthetic carbonated apatites and dental enamel. *Australian Journal of Chemistry*, 35, 715–727, <https://doi.org/10.1071/CH9820715>.

Nokhrin, S.M., Pan, Y.M., Weil, J.A., and Nilges, M.J. (2005) Multifrequency EPR study of radiation-induced defects in chlorapatite. *Canadian Mineralogist*, 43, 1581–1588, <https://doi.org/10.2113/gscanmin.43.5.1581>.

Prener, J.S., Piper, W.W., and Chrenko, R.M. (1969) Hydroxide and oxide impurities in calcium halophosphates. *Journal of Physics and Chemistry of Solids*, 30, 1465–1481, [https://doi.org/10.1016/0022-3697\(69\)90209-1](https://doi.org/10.1016/0022-3697(69)90209-1).

Reimann, B., Buchhold, K., Vaupel, S., Brutschy, B., Havlas, Z., Špirko, V., and Hobza, P. (2001) Improper, blue-shifting hydrogen bond between fluorobenzene and fluoroform. *The Journal of Physical Chemistry A*, 105, 5560–5566, <https://doi.org/10.1021/jp003726q>.

Schettler, G., Gottschalk, M., and Harlov, D.E. (2011) A new semi-micro wet chemical method for apatite analysis and its application to the crystal chemistry of fluorapatite-chlorapatite solid solutions. *American Mineralogist*, 96, 138–152, <https://doi.org/10.2138/am.2011.3509>.

Shannon, R.D. (1976) Revised effective ionic-radii and systematic studies of interatomic distances in halides and chalcogenides. *Acta Crystallographica Section A*, 32, 751–767, <https://doi.org/10.1107/S0567739476001551>.

Stormer, J.C., Pierson, M.L., and Tacker, R.C. (1993) Variation of F-X-ray and Cl-X-ray Intensity due to anisotropic diffusion in apatite during electron-microprobe analysis. *American Mineralogist*, 78, 641–648.

Tacker, R.C. (2004) Hydroxyl ordering in igneous apatite. *American Mineralogist*, 89, 1411–1421, <https://doi.org/10.2138/am-2004-1008>.

Yasukawa, A., Ueda, E., Kandori, K., and Ishikawa, T. (2005) Preparation and characterization of carbonated barium-calcium hydroxyapatite solid solutions. *Journal of Colloid and Interface Science*, 288, 468–474.

Yu, H.G., Zhang, H.L., Wang, X.M., Gu, Z.W., Li, X.D., and Deng, F. (2007) Local structure of hydroxy-peroxy apatite: A combined XRD, FT-IR, Raman, SEM, and solid-state NMR study. *Journal of Physics and Chemistry of Solids*, 68, 1863–1871, <https://doi.org/10.1016/j.jpcs.2007.05.020>.

Zhou, J.M., Zhang, X.D., Chen, J.Y., Zeng, S.X., and Degroot, K. (1993) High-temperature characteristics of synthetic hydroxyapatite. *Journal of Materials Science: Materials in Medicine*, 4, 83–85, <https://doi.org/10.1007/BF00122983>.

Zhukova, E.S., Torgashev, V.I., Gorshunov, B.P., Lebedev, V.V., Shakurov, G.S., Kremer, R.K., Pestjakov, E.V., Thomas, V.G., Fursenko, D.A., Prokhorov, A.S., and Dressel, M. (2014) Vibrational states of a water molecule in a nano-cavity of beryl crystal lattice. *The Journal of Chemical Physics*, 140, 224317, <https://doi.org/10.1063/1.4882062>.

MANUSCRIPT RECEIVED MAY 9, 2023

MANUSCRIPT ACCEPTED FEBRUARY 27, 2024

ACCEPTED MANUSCRIPT ONLINE MARCH 28, 2024

MANUSCRIPT HANDLED BY YASSIR A. ABDU

Endnote:

¹Deposit item AM-24-129059. Online Materials are free to all readers. Go online, via the table of contents or article view, and find the tab or link for supplemental materials.